Available online at www.sciencedirect.com
ScienceDirect
Computational Materials Science 38 (2006) 303–315
COMPUTATIONAL MATERIALS SCIENCE
www.elsevier.com/locate/commatsci

Computational aspects of the Cosserat finite element analysis of localization phenomena

E. Sharbati, R. Naghdabadi *

Department of Mechanical Engineering, Sharif University of Technology, P.O. Box 11365-9567 Tehran, Iran

Received 20 October 2005; received in revised form 1 March 2006; accepted 10 March 2006

Abstract

The computational aspects of the finite element solution procedure based on the Cosserat theory are studied for some elastic–plastic problems, in which the localization occurs. For this purpose, the equations of the Cosserat elasto-plasticity, which include effects of couple stress, micro-rotation and length scale, are presented. The Cosserat finite element formulation is derived and an algorithm for the solution procedure is proposed. For the elastic–plastic problems considered here, the mesh-independency of the Cosserat-based results is quantified and effects of the internal length and Cosserat material parameter a are investigated on the results. Also, the influence of the internal length on the convergence rate of the solution procedure is studied. A comparison of the results based on the Cosserat theory and those based on the couple stress and classical theories is presented. In addition, the results of the Cosserat theory are compared with the experimental data available in the literature. It is shown that in spite of an additional degree of freedom for each node in the Cosserat theory, the computational effort for the solution procedure in this theory is less than the classical theory. Also, convergence rate is affected more significantly by decrease of the internal length in finer discretizations.

Keywords: Cosserat theory; Finite element analysis; Computational effort; Elastic–plastic analysis

1. Introduction

Classical theory of plasticity fails to give reasonable results in problems in which the plastic deformation confines to local domains. Also, the results obtained by conventional finite element, which is based on the classical continuum mechanics and plasticity, fail to predict the size of such domains correctly. In fact, by decreasing the size of elements used for discretizing the body, the size of the localized domain also decreases. In other words, the solution is mesh dependent [1]. So many works have been done to model the localization phenomena correctly [1–4]. One way to overcome this problem is to use non-classical theories, which include couple stresses as well as a measure of length scale. A variety of these theories exist and one of the most general forms of them is the Cosserat theory. Other theories of this type are proposed in [1,4,5].

One of the most important features of the Cosserat continuum theory that makes it different from the classical one is the insertion of couple stresses, which makes the stress tensor non-symmetric. As a consequence, in addition to body forces, the Cosserat theory is capable of including body couples, which are ignored in the classical theory. Furthermore, by considering a new degree of freedom for each particle called micro-rotation, the strain tensor becomes non-symmetric too [6]. This new degree of freedom states that a particle in a Cosserat continuum is micro-polar and thus can rotate independently from the whole body, which may have a macro-rotation. In addition, when deriving constitutive equations based on the Cosserat theory, some new parameters including the internal length appear in these equations [6]. This parameter has a great role in succession of the Cosserat theory for modeling the problems that the classical theory is not capable of modeling them.

* Corresponding author. Tel.: +98 21 66005716; fax: +98 21 66000021.
E-mail address: naghdabd@sharif.edu (R. Naghdabadi).

0927-0256/$ - see front matter © 2006 Elsevier B.V. All rights reserved.
doi:10.1016/j.commatsci.2006.03.003

The Cosserat theory was first proposed by the Cosserat brothers in 1909 [7]. The concise derivation of basic equations of Cosserat elasticity has been presented by Mindlin in [6]. He has also obtained a solution including the displacement field for the linear equations of an elastic Cosserat continuum. The stress distribution around a circular hole in an infinite plate under uniaxial tension has been obtained by Neuber in [8] using the Cosserat theory. It has been shown that the equilibrium equations of the Cosserat elasticity can be written as a 14-dimensional coupled linear system of differential equations of first order [9].

The early works on finite element analysis based on the Cosserat theory are those done by Baluch et al. [10] and Nakamura et al. [11] in which a simple three-node triangle element with three degrees of freedom at each node has been proposed. Three higher-order triangle finite elements for two-dimensional analysis based on the Cosserat elasticity have been recently presented by Providas and Kattis [12]. In this work, the field equations of the plane Cosserat elasticity are expressed in oblique rectilinear coordinates. The Cosserat theory has also been employed by Nadler and Rubin to formulate a 3-D finite element for dynamic analysis in nonlinear elasticity [13]. In addition, three higher-order finite elements for elastic analysis of shells have been proposed by Jog [14].

The elastic–plastic modeling of localization phenomena has been done by Chambon et al. [4]. They have proposed two plastic second gradient models including Cosserat second gradient and local second gradient models. Cramer et al. have employed both classical and Cosserat theories for adaptive finite element analysis in associated and non-associated plasticity [3]. They have shown that the Cosserat theory is superior to the classical theory in modeling of localization phenomena. An elastic–plastic finite element analysis software has been presented by Cerrolazaa et al. [15] for modeling of blocky structures by use of the Cosserat theory.

In this paper, the basic equations of Cosserat elasto-plasticity including kinematic and stress relations, constitutive equations, yield criterion, flow rule and hardening rule, which are different from those of the classical theory, are presented. These relations are used to derive the Cosserat finite element formulation for a four-node quadrilateral element with three degrees of freedom at each node including one rotational and two translational degrees of freedom. A computer program based on the Cosserat finite element formulation has been prepared and the computational aspects of the solution procedure for some common elastic–plastic analyses are studied. The mesh-independency of the Cosserat-based results is quantified for the elastic–plastic problems analyzed here. In addition, effects of the internal length and the Cosserat material parameter a on the convergence rate of the solution procedure are investigated. Finally, the results based on the Cosserat finite element formulation are compared with the results of the couple stress and classical theories available in the literature.

2. Basic equations of Cosserat elasticity

In order to express motion of a particle in a Cosserat continuum, we need to introduce the vector of micro-rotation $\boldsymbol{\phi}$ in addition to the well-known displacement vector $\mathbf{u}$. The micro-rotation vector is independent of the classical macro-rotation, which is the curl of the displacement vector. The strain tensor components are functions of the displacement and micro-rotation as follows [12]:

$$\varepsilon_{ij} = \frac{\partial u_i}{\partial x_j} + e_{ijk}\varphi_k \tag{1}$$

where u_i and φ_k are the components of displacement and micro-rotation vectors, respectively. Also, e_{ijk} is the component of permutation tensor. From Eq. (1), it is clear that the strain tensor is not symmetric. The gradient of the micro-rotation vector is known as micro-curvature tensor and is defined in the form of:

$$\kappa_{ij} = \frac{\partial \varphi_j}{\partial x_i} \tag{2}$$

where κ_{ij} is the component of the micro-rotation tensor. While the strain tensor ε is work conjugate to the stress tensor σ, the curvature tensor κ is work conjugate to the couple stress tensor m [6]. The constitutive equations governing an elastic Cosserat medium are:

$$\sigma_{ij} = D_{ijkl}\varepsilon_{kl} \tag{3}$$

$$m_{ij} = M_{ijkl}\kappa_{kl} \tag{4}$$

where m_{ij} is the component of the couple stress tensor. For the case of an isotropic material we have [12]

$$D_{ijkl} = G\left[(1+a)\delta_{ik}\delta_{jl} + (1-a)\delta_{il}\delta_{jk} + \frac{2v}{1-2v}\delta_{ij}\delta_{kl}\right] \tag{5}$$

$$M_{ijkl} = 4Gl^2(\delta_{ik}\delta_{jl} + b\delta_{il}\delta_{jk} + c\delta_{ij}\delta_{kl}) \tag{6}$$

where G is the shear modulus, v is the Poisson's ratio, l is the internal length, δ_{ij} is the Kronecker delta, and a, b, and c are Cosserat material constants. Also, equations of equilibrium governing a Cosserat continuum are as follows:

$$\frac{\partial \sigma_{ji}}{\partial x_j} + X_i = 0 \tag{7}$$

$$\frac{\partial m_{ji}}{\partial x_j} + e_{ijk}\sigma_{jk} + Y_i = 0 \tag{8}$$

where X_i and Y_i are the components of the body force and body couple vectors, respectively. Ignoring the couple stresses and body couples in (8), the equilibrium equations are reduced to the classical form in which the stress tensor is symmetric. Eqs. (1)–(8) are the basic equations for the Cosserat elasticity.

Since in this paper we are concerned with plane problems, these equations should be reduced to two dimensional forms, i.e. in x–y plane. In the case of plane strain since there is no motion in the z-direction, u_z, φ_x, and φ_y vanish. Consequently, due to vanishing the gradient of u_x

and u_y along the z-direction, the non-zero components of the strain tensor are ε_{xx}, ε_{yy}, ε_{xy}, and ε_{yx} in accordance with Eq. (1), and the curvature components remaining are κ_{xz} and κ_{yz} in accordance with Eq. (2). Introducing the non-zero strains and curvatures into Eqs. (3)–(6), the non-zero components of the stress tensor are σ_{xx}, σ_{yy}, σ_{xy}, σ_{yx} and σ_{zz}, while the only non-zero components of the couple stress tensor are m_{xz} and m_{yz}. Thus, the constitutive equation for the plane Cosserat elasticity is obtained as

$$\vec{\sigma} = C^{\mathrm{e}}\vec{\varepsilon}^{\mathrm{e}} \tag{9}$$

where $\vec{\sigma}$, $\vec{\varepsilon}^{\mathrm{e}}$ and C^{e} are defined as follows:

$$\vec{\sigma} = \begin{bmatrix} \sigma_{xx} & \sigma_{yy} & \sigma_{zz} & \sigma_{xy} & \sigma_{yx} & m_{xz} & m_{yz} \end{bmatrix}^{\mathrm{T}} \tag{10a}$$

$$\vec{\varepsilon}^{\mathrm{e}} = \begin{bmatrix} \varepsilon^{\mathrm{e}}_{xx} & \varepsilon^{\mathrm{e}}_{yy} & \varepsilon^{\mathrm{e}}_{zz} & \varepsilon^{\mathrm{e}}_{xy} & \varepsilon^{\mathrm{e}}_{yx} & \kappa^{\mathrm{e}}_{xz} & \kappa^{\mathrm{e}}_{yz} \end{bmatrix}^{\mathrm{T}} \tag{10b}$$

$$C^{\mathrm{e}} = G\begin{bmatrix} \frac{2(1-\nu)}{1-2\nu} & \frac{2\nu}{1-2\nu} & \frac{2\nu}{1-2\nu} & 0 & 0 & 0 & 0 \\ & \frac{2(1-\nu)}{1-2\nu} & \frac{2\nu}{1-2\nu} & 0 & 0 & 0 & 0 \\ & & \frac{2(1-\nu)}{1-2\nu} & 0 & 0 & 0 & 0 \\ & & & 1+a & 1-a & 0 & 0 \\ & \textit{Sym.} & & & 1+a & 0 & 0 \\ & & & & & 4l^2 & 0 \\ & & & & & & 4l^2 \end{bmatrix} \tag{11}$$

It is noted that the dimensionless parameters b and c do not enter the plane form of the Cosserat constitutive equations. However, these parameters exist in the general form of the stress–strain relations. On the other hand, the dimensionless parameter a which remains in the equations, is a Cosserat elasticity parameter. The constitutive Eq. (11) has appeared with different multiplier in the couple stress–curvature relation in the literature. For instance, this multiplier which is 4 in Eq. (11) is replaced by 2 in [16] and is equal to 1 in [3]. The distinction of this multiplier renders different definitions of the length scale l used in these works. An elastic solution for the Cosserat medium can be found in [8] while a stress function for the Cosserat continuum is presented in [6].

3. Elastic–plastic formulation for a Cosserat medium

In order to derive elastic–plastic relations in the Cosserat theory, use of the basic equations of Cosserat plasticity is required. These equations include yield criterion, flow rule and hardening rule. The elastic and plastic equations of the Cosserat theory are used to form elastic–plastic relations.

The yield surface in the Cosserat theory is used in the same form as in the classical theory [15]

$$F = \sqrt{3J_2} - \sigma_{\mathrm{y}}(K) = 0 \tag{12}$$

where σ_{y} is the current yield stress which is a function of the hardening parameter K, such as equivalent plastic strain. In the classical theory, the parameter J_2 is the second invariant of the deviatoric part of the stress tensor. This parameter should be generalized to cover the effect of couple stress and the non-symmetric nature of the stress tensor in the Cosserat theory. For this purpose, a new definition of J_2 is used in the form

$$J_2 = H_1 S_{ij}S_{ij} + H_2 S_{ij}S_{ji} + H_3\frac{m_{ij}m_{ij}}{l^2} \tag{13}$$

where H_1, H_2, and H_3 are arbitrary parameters and S_{ij} is the component of the deviatoric part of the stress tensor. Eq. (13) should be consistent with the classical form of J_2 (where $m_{ij} = 0$ and $S_{ij} = S_{ji}$), thus we should have

$$H_1 + H_2 = 1/2 \tag{14}$$

Since we are concerned with the small deformations, the decompositions of the rates of strain and curvature are:

$$\dot{\varepsilon}_{ij} = \dot{\varepsilon}^{\mathrm{e}}_{ij} + \dot{\varepsilon}^{\mathrm{p}}_{ij}, \quad \dot{\kappa}_{ij} = \kappa^{\mathrm{e}}_{ij} + \kappa^{\mathrm{p}}_{ij} \tag{15}$$

where the superscripts 'e' and 'p' denote the elastic and plastic parts, respectively.

The flow rule for the Cosserat plasticity is the same as the classical theory except that it should be generalized to cover the relation for the plastic part of the curvature in addition to the plastic part of the strain [3]. Using associated plasticity, the flow rule for the strain and curvature rates are as follows:

$$\dot{\varepsilon}^{\mathrm{p}}_{ij} = \dot{\lambda}\frac{\partial F}{\partial \sigma_{ij}} \tag{16}$$

$$\dot{\kappa}^{\mathrm{p}}_{ij} = \dot{\lambda}\frac{\partial F}{\partial m_{ij}} \tag{17}$$

where F is the yield surface.

The final step is to use elastic and plastic relations to derive an equation which relates the strain and curvature rates to the stress and couple stress rates. Differentiating Eq. (9), and using Eq. (15), we obtain:

$$\dot{\vec{\sigma}} = C^{\mathrm{e}}(\dot{\vec{\varepsilon}} - \dot{\vec{\varepsilon}}^{\mathrm{p}}) \tag{18}$$

Substitution of Eqs. (16) and (17) into Eq. (18) leads to:

$$\dot{\vec{\sigma}} = C^{\mathrm{e}}(\dot{\vec{\varepsilon}} - \dot{\lambda}\vec{f}) \tag{19}$$

where $\vec{f}$ is the normal vector to the yield surface whose components are determined using Eqs. (16) and (17). Using the consistency condition ($\mathrm{d}F = 0$) together with Eq. (19), $\dot{\lambda}$ is found as follows:

$$\dot{\lambda} = \frac{\vec{f}^{\mathrm{T}}C^{\mathrm{e}}\dot{\vec{\varepsilon}}}{H + \vec{f}^{\mathrm{T}}C^{\mathrm{e}}f} \tag{20}$$

where H is the plastic modulus. Substituting Eq. (20) into (19) and rewriting the result in a more useful form, we obtain:

$$\dot{\vec{\sigma}} = C^{\mathrm{e}}\left(I - \frac{\vec{f}\vec{f}^{\mathrm{T}}C^{\mathrm{e}}}{H + \vec{f}^{\mathrm{T}}C^{\mathrm{e}}\vec{f}}\right)\dot{\vec{\varepsilon}} = C^{\mathrm{ep}}\dot{\vec{\varepsilon}} \tag{21}$$

Eq. (21) represents a general form of elastic–plastic stiffness matrix in the case of isotropic hardening for a Cosserat material.

The elastic–plastic relations derived in this part (Eqs. (12)–(21)) are for three dimensional case. For the plane Cosserat theory, J_2 in the yield criterion (Eq. (13)) reduces to:

$$J_2 = (H_1+H_2)(S_{xx}^2+S_{yy}^2+S_{zz}^2)+H_1(S_{xy}^2+S_{yx}^2) + 2H_2S_{xy}S_{yx}+H_3\left(\frac{m_{xz}^2}{l^2}+\frac{m_{yz}^2}{l^2}\right) \tag{22}$$

Furthermore, for the plane Cosserat theory, the vectors $\dot{\vec{\sigma}}$ and $\dot{\vec{\varepsilon}}$, and matrix C^e in Eq. (21) are the same as the ones in Eqs. (10) and (11) while the vector $\vec{f}$ is [15]:

$$\vec{f} = \frac{\sqrt{3}}{2\sqrt{J_2}}\frac{\partial J_2}{\partial \vec{\sigma}} = \frac{\sqrt{3}}{2\sqrt{J_2}}\begin{bmatrix} 2(H_1+H_2)S_{xx} \\ 2(H_1+H_2)S_{yy} \\ 2(H_1+H_2)S_{zz} \\ 2(H_1S_{xy}+H_2S_{yx}) \\ 2(H_1S_{yx}+H_2S_{xy}) \\ 2H_3\dfrac{m_{xz}}{l^2} \\ 2H_3\dfrac{m_{yz}}{l^2} \end{bmatrix} \tag{23}$$

Eqs. (21)–(23) are the elastic–plastic relations for the plane Cosserat theory. These equations together with the elastic equations are required for the finite element formulation of elastic–plastic analysis using the plane Cosserat theory.

4. Finite element formulation

Considering an arbitrary element in the x–y plane (see Fig. 1), the displacement and micro-rotation fields are expressed by

$$u_x = \vec{N}^{\mathrm{T}}\vec{u}_x^n, \quad u_y = \vec{N}^{\mathrm{T}}\vec{u}_y^n, \quad \varphi_z = \vec{N}^{\mathrm{T}}\vec{\varphi}_z^n \tag{24}$$

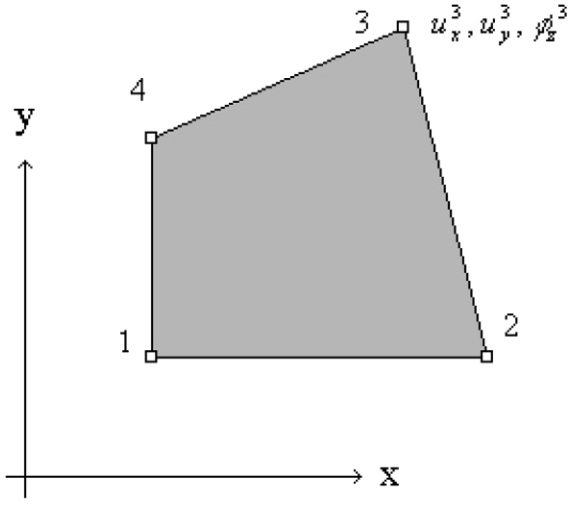

Fig. 1. An arbitrary four-node quadrilateral finite element with three degrees of freedom at each node u_x^3, u_y^3, ϕ_z^3.

where vectors $\vec{u}_x^n$, $\vec{u}_y^n$, and $\vec{\varphi}^n$ contain nodal x- and y-displacements and micro-rotation of an element, respectively. The superscript 'n' represents vectors containing nodal degrees of freedom. Also, vector $\vec{N}$ contains the element shape functions. The same shape functions are used for both displacements and micro-rotation in Eq. (24) [12]. Substituting Eq. (24) into Eqs. (1) and (2), the relation for the strain is written as follows:

$$\vec{\varepsilon} = B\vec{u}^n \tag{25}$$

where vector $\vec{u}^n$ is the vector of nodal displacements and micro-rotations. Also, B matrix represents the (strain, curvature)–(displacement, micro-rotation) relations

$$B = \begin{bmatrix} \dfrac{\partial \vec{N}^{\mathrm{T}}}{\partial x} & \vec{0} & \vec{0} \\ \vec{0} & \dfrac{\partial \vec{N}^{\mathrm{T}}}{\partial y} & \vec{0} \\ \vec{0} & \vec{0} & \vec{0} \\ \dfrac{\partial \vec{N}^{\mathrm{T}}}{\partial y} & \vec{0} & -\vec{N}^{\mathrm{T}} \\ \vec{0} & \dfrac{\partial \vec{N}^{\mathrm{T}}}{\partial x} & \vec{N}^{\mathrm{T}} \\ \vec{0} & \vec{0} & \dfrac{\partial \vec{N}^{\mathrm{T}}}{\partial x} \\ \vec{0} & \vec{0} & \dfrac{\partial \vec{N}^{\mathrm{T}}}{\partial y} \end{bmatrix}, \quad \vec{\varepsilon} = \begin{bmatrix} \varepsilon_{xx} \\ \varepsilon_{yy} \\ \varepsilon_{zz} \\ \varepsilon_{xy} \\ \varepsilon_{yx} \\ \kappa_{xz} \\ \kappa_{yz} \end{bmatrix} \tag{26}$$

Since the third row of B matrix contains zero components, ε_{zz} vanishes. Thus, such form of B matrix implies the case of plane strain.

Considering the principle of virtual work, the weak form of the equilibrium equation is written as follows:

$$\int_V B^{\mathrm{T}}\vec{\sigma}\,\mathrm{d}V = \int_V N^{\mathrm{T}}\vec{p}\,\mathrm{d}V + \int_S N^{\mathrm{T}}\vec{t}\,\mathrm{d}s \tag{27}$$

where the components of vector $\vec{p}$ are body forces and body couples. Also, the components of vector $\vec{t}$ are surface forces and surface couples. Following the same procedure as used in the classical finite element method [17], the element stiffness matrix, $K^{(e)}$ is derived in the form

$$K^{(e)} = \int_V B^{\mathrm{T}}CB\,\mathrm{d}V \tag{28}$$

where C is the stress–strain matrix. For the elastic case, matrix C equals C^e and is evaluated from Eq. (11), while it is computed from Eq. (21) for the elastic–plastic case.

The element used in this paper is the standard four-node quadrilateral element. Since the shape functions in this element are functions of natural coordinates, we need to compute the inverse of Jacobian matrix to evaluate B matrix. Furthermore, Gauss quadrature method is used for numerical integration of Eq. (28). A full discussion on this element and numerical integration can be found in [17].

5. Analysis methodology

The methodology used for elastic–plastic finite element analysis based on the classical theory should be generalized to be used for the Cosserat theory. Since the constitutive equations for plastic deformation are path dependent, the equations governing a continuum in plastic region are nonlinear. In this paper, the Newton–Raphson algorithm is used to solve the nonlinear governing equations. As a consequence, the procedure used for solving elastic–plastic problems is an incremental-iterative one. For this purpose, in each load increment, an iterative procedure is used to obtain a stress field which satisfies the equilibrium equations. At the end of each increment, the displacement–micro-rotation and the stress–couple stress fields are updated. To obtain results with reasonable accuracy use of adequate increments is essential.

There are different approaches for using Newton–Raphson algorithm in the elastic–plastic analysis. The algorithm used in this paper involves the following steps:

1. Start the current increment (load step) with the displacement–micro-rotation and the stress–couple stress fields known from the previous converged increment.
2. Compute the iterative displacements–micro-rotation $\delta\vec{p}$ using the equation

$$\delta\vec{p} = -K_t^{-1}\vec{g} \tag{29}$$

where K_t is the tangent stiffness matrix and $\vec{g}$ represents the out of balance forces computed from the relation

$$\vec{g} = \int_V B^{\mathrm{T}}\vec{\sigma}\,\mathrm{d}V - \int_V N^{\mathrm{T}}\vec{p}\,\mathrm{d}V - \int_S N^{\mathrm{T}}\vec{t}\,\mathrm{d}s \tag{30}$$

3. Update the incremental displacements–micro-rotations ($\Delta\vec{p}$) by adding $\delta\vec{p}$ to the current value of $\Delta\vec{p}$.
4. Compute the incremental strains–curvature corresponding to the incremental displacements–micro-rotations using the kinematic equations.
5. Compute the incremental stresses–couple stresses using $\Delta\vec{\sigma} = C^{\mathrm{ep}}\Delta\vec{\varepsilon}$ or preferably integrating the rate constitutive equations [18].
6. Update the stresses–couple stresses using $\vec{\sigma} = \vec{\sigma}_0 + \Delta\vec{\sigma}$, where $\vec{\sigma}_0$ represents the vector of the stresses–couple stresses at the end of the last increment.
7. Advance to the next increment, if the convergence criterion is satisfied.

The convergence criterion may be the force-based and/or the displacement-based. The force-based convergence criterion is expressed in the form

$$\|\vec{g}\| < \bar{\varepsilon} \tag{31}$$

where $\bar{\varepsilon}$ is a small number. The displacement-based convergence criterion is written as follows:

$$\|\delta\vec{p}\| < \bar{\varepsilon} \tag{32}$$

The main advantage of this algorithm is that in each iteration, the stresses are updated using the stresses of the last converged increment. On the other hand, since C^{ep} is a function of stress (or in other words the constitutive equation has a rate form), we may need to use some sub-increments to integrate the rate equation in step 5, and consequently this step is usually a time consuming process. Although use of the sub-increments improves the precision of the updated stresses in step 5, it cannot remove the error completely. To be more precise, the updated state of stress will usually lie out of the yield surface and we need to use some techniques to return it back to the yield surface. Some of these techniques are backward and forward Euler methods, use of sub-increments and the radial return method which are explained in detail in [18]. The method used in this paper is the forward Euler method.

The finite element formulations presented in the previous sections together with this algorithm are sufficient to write a computer implementation for the Cosserat elastic–plastic finite element analysis. The computer implementation prepared is capable of analyzing an arbitrary plate under arbitrary loadings including forces, moments, displacements, micro-rotations, body forces and body couples in the cases of plane stress and plane strain. The program is also capable of performing both full Newton–Raphson and modified Newton–Raphson algorithms.

6. Results and discussion

In this section, the computer program prepared for the Cosserat finite element analysis is used to study the computational aspects of finite element analysis based on the Cosserat theory. For this purpose, some elastic and elastic–plastic problems are solved and the numerical results are presented and compared with the results obtained in other works [1,12]. In order to verify the elastic results, a number of elastic analyses are carried out on a square plate with a relatively small hole and the results are compared with those presented by Providas and Kattis in [12]. For elastic–plastic analyses, the tension of a rectangular plate with softening material is considered for different finite element discretizations as well as different Cosserat material parameters.

6.1. Elastic analyses

Consider a square plate of 32.4 mm size length, containing a relatively small circular hole of radius r in the center and bearing a uniform tension of 1 N/mm^2 in one direction. The plate has been analyzed for $r = 0.216$ mm and $r = 0.864$ mm with different values of the internal length l and material parameter a. The maximum stress occurring around the hole are presented in Table 1 for different values of l and a.

The results presented in Table 1 are compared with the numerical results obtained in [12] and the analytical solution for different values of the parameter a and internal

Table 1
The maximum stress in a plate containing a relatively small circular hole under uniaxial tension when different values of the internal length l and material parameter a are used

a	Analytical [8]	Results of [12]	Error % in [12]	This work	Our error (%)
(a) r = 0216 mm, r/l = 1.063, v = 0.3, mesh 8 × 22					
0	3	2.867	4.4	3.106	3.53
0.0667	2.849	2.753	3.4	2.948	3.47
0.3333	2.555	2.516	1.5	2.631	2.97
1.2857	2.287	2.269	0.8	2.328	1.79
4.2632	2.158	2.103	2.6	2.173	0.70
a	Analytical [8]	Results of [12]	Error % in [12]	This work	Our error (%)
(b) r = 0.216 mm, r/l = 10.63, v = 0.3, mesh 8 × 22					
0	3	2.867	4.4	3.106	3.53
0.0667	2.956	2.833	4.2	3.056	3.38
0.3333	2.935	2.809	4.3	3.023	3.00
12857	2.927	2.761	5.7	2.984	1.95
4.2632	2.923	2.633	9.9	2.906	0.58
r/1	Analytical [8]	Results of [12]	Error % in [12]	This work	Our error (%)
(c) r = 0.864 mm, a = 1/3, v = 0.3, mesh 8 × 15					
1	2.549	2.524	1.0	2.639	3.53
2	2.641	2.599	1.6	2.733	3.48
3	2.719	2.661	2.1	2.814	3.49
4	2.779	2.709	2.5	2.877	3.53
6	2.857	2.77	3.1	2.960	3.61
8	2.902	2.804	3.4	3.008	3.65
10	2.929	2.824	3.6	3.037	3.69

(a) Different values of a for $r/l = 1.063$. (b) Different values of a for $r/l = 10.63$. (c) Different values of the internal length l for $a = 1/3$.

length l presented in [8]. The pattern of the meshes used for these analyses are approximately the same as [12] except that the element used is four-node quadrilateral. The error values presented in Table 1 are computed with respect to the analytical solution. A glance at the table indicates that the finite element elastic results obtained in this work are in good agreement with the analytical solution. Also, the maximum stresses obtained by the use of the quadrilateral element are greater than those of the analytical solution for all values of the internal length l and material parameter a. On the other hand, the maximum stresses obtained by the application of triangle element are smaller than the analytical solution. In addition, it is noted that when the quadrilateral element is used, the increase in the Cosserat parameter a causes a reduction in error.

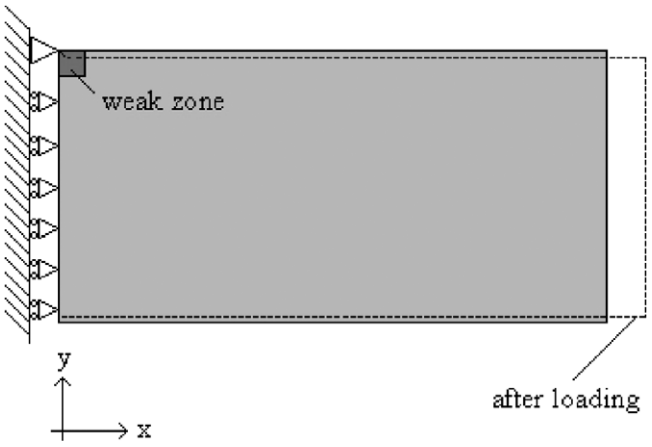

Fig. 2. The geometry and boundary conditions of the plate used in elastic–plastic analyses. The right side of the plate is subjected to a displacement-control load.

6.2. Elastic–plastic analyses

For the elastic–plastic analyses a rectangular plate of 60 mm width and 120 mm height is horizontally (i.e. x-direction) fixed at one end while the other end is subjected to a given horizontal displacement (the load is a displacement control one). The geometry and boundary conditions used for the plate are shown in Fig. 2. In addition, the upper left corner of the plate is vertically fixed. The material properties are: Young modulus $E = 4000$ N/mm^2, Poisson's ratio $v = 0.49$, plastic modulus $H = -0.03$E, and initial yield stress $\sigma_{y0} = 100$ N/mm^2. In these analyses, various values for the internal length l and material parameter a are used to investigate effects of these parameters. For the sake of comparison, the geometry, material properties and loadings used in this problem are the same as the ones used in [1] in which the couple stress theory is employed.

One way to trigger the localization is to assume a material imperfection somewhere in the plate. In this work, a lower value of initial yield stress of 98 N/mm^2 is assigned to the weak zone as shown in Fig. 2. In addition, to show the shortcoming of the classical theory in the modeling of the localization phenomena, different finite element discretizations are used.

Fig. 3 illustrates the plastic zone obtained for the problem when the classical and Cosserat theories with different discretizations are used. The results are for the state of plane strain and subjecting the right side of the plate to a horizontal displacement of 4.2 mm. As it is expected, the plastic zone obtained for the classical theory (Fig. 3a) becomes narrower as the discretization refines. In fact, the plastic zone is two elements wide for all discretizations which shows the mesh-dependency of the results based on the classical theory. On the other hand, the plastic zone obtained for the Cosserat theory (Fig. 3b) approximately remains unchanged when discretization refines.

The mesh-independency of the results obtained based on the Cosserat theory, shows that they can be acceptable. However, in order to validate the results, it is useful to compare them with the experimental data. Vardoulakis et al. [19] have done experimental analyses in granular materials. They have shown that the localized zone is approximately 16 times the average grain size. The first consequence of their findings is that the classical results are not valid when localization occurs. Also, if we consider the internal length as the average grain size and apply the findings of Vardoulakis et al. [19], the localized zone for the internal length of 2 mm is 32 mm. This value is close to the localized zone size obtained here, which is approximately 36 mm as shown in Fig. 3. Thus, the results based on the Cosserat theory are in good agreement with the experimental results presented in [19].

The limitation of the classical theory in analyzing localization phenomena does not confine to predicting the plastic zone incorrectly. As a matter of fact, the solution throughout the whole domain is mesh-dependent. Fig. 4 renders the force–displacement charts for this problem when the classical, Cosserat and couple stress theories are used with various discretizations. The results for the couple stress theory have been obtained by Ristinmaa and Vecchi

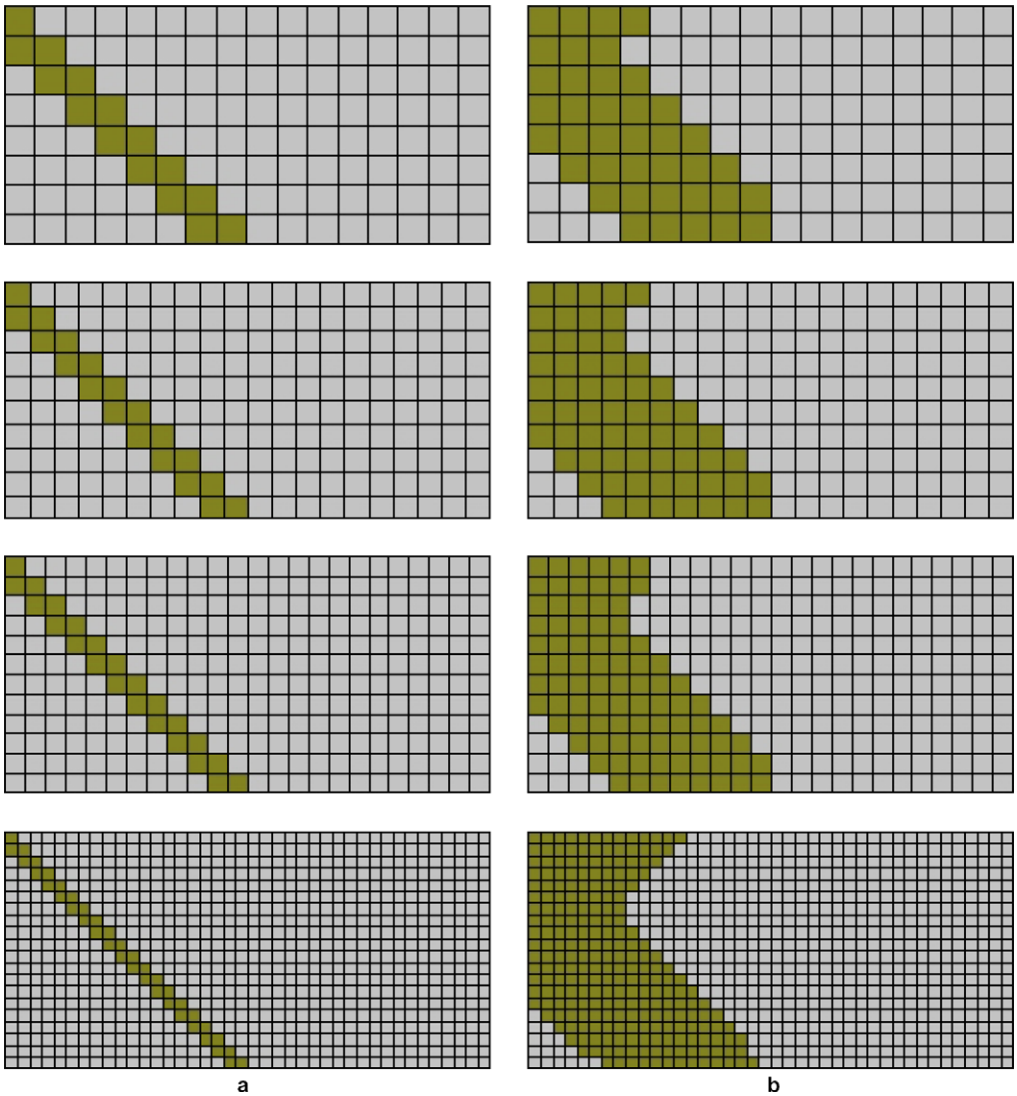

Fig. 3. Plastic zone for the plate subjected to a horizontal displacement of 4.2 mm at the right end. The meshes are 8×16, 10×20, 12×24, 20×40 (a) Classical theory. (b) Cosserat theory with internal length $l = 2$ and Cosserat parameter $a = 0.5$.

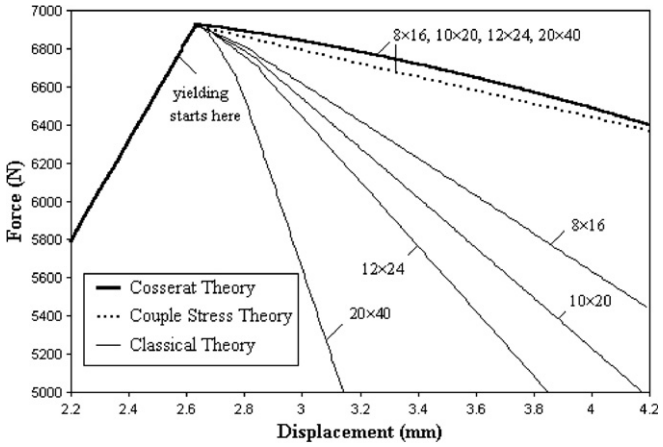

Fig. 4. Force–displacement curves for different discretizations of the plate when Cosserat, couple stress [1] and classical theories are used. The internal length is 2 mm.

[1]. The vertical axis in these charts represents the force in the x-direction needed at the right side of the plate to produce the corresponding displacement. In other words, it is the sum of nodal reactions at the right side of the plate. As shown in Fig. 4, the classical theory does not give a unique solution for different element sizes beyond the peak force value. It is noted that the curves corresponding to different discretizations coincide in the elastic as well as the elastic–plastic region before the occurrence of the instability. On the other hand, the force–displacement curves for different element sizes in Fig. 4 exactly coincide for the Cosserat as well as the couple stress theories. Considering either of the curves in Fig. 4, it is seen that none of the curves of the classical results coincide with them.

In accordance with the results obtained by the classical theory, it is concluded that the Cosserat theory is more successful than the classical theory in modeling of localization. Furthermore, the couple stress theory presented in [1] gives somehow the same results as the Cosserat theory (the couple stress results are mesh-independent). Nevertheless, the results obtained by these two theories are not exactly the same (refer to Fig. 5b for instance). This difference is more obvious when smaller values of internal length are used: in accordance with force–displacement diagram for $l = 1$ presented in [1], the force corresponding to displacement 4.2 mm for the couple stress theory is approximately 5300 N while this value for the Cosserat theory is 5850 N. On the other hand, this value for $l = 2$ mm is 6350 N and 6400 N for couple stress and Cosserat theories, respectively. Thus, it is concluded that the difference between the mentioned theories are more for $l = 1$. The difference between the two theories is also reflected in Fig. 5, which is the deformed shape of the plate subjected to a 4.2 mm displacement of the boundary when the internal length is 1 mm. Fig 5(b) has been presented in [1] by use of the couple stress theory. A comparison of the two patterns shows that the Cosserat theory gives a smoother deformed pattern. To be more precise, the localized

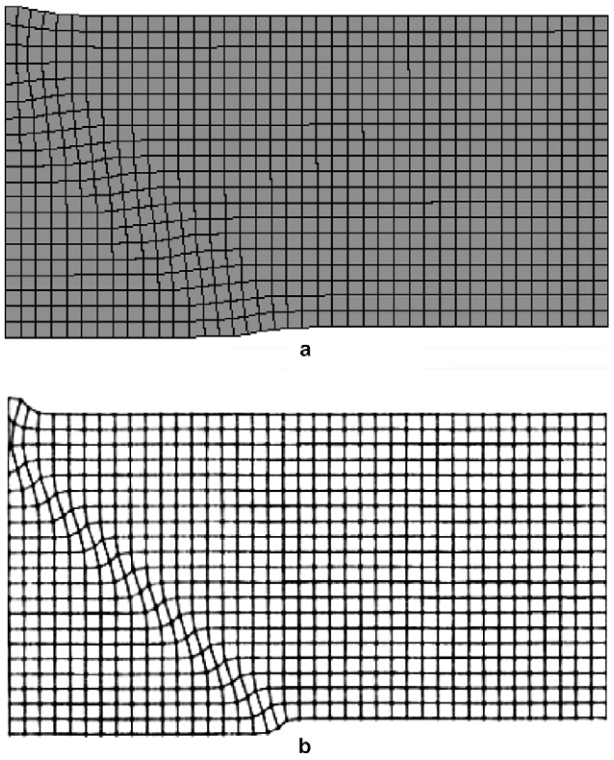

Fig. 5. Comparison between the deformed shape of the plate obtained by using the Cosserat and couple stress theories. The right side is subjected to 4.2 mm horizontal displacement and internal length is 1 mm. (a) Result for the Cosserat theory, parameter a has a value of 0.5. (b) Result for the couple stress theory [1].

domain is approximately two elements wide in couple stress theory while it is about six elements wide in the Cosserat theory.

7. Computational aspects and effects of Cosserat parameters

7.1. Computational efforts in the Cosserat theory

Although there is one additional degree of freedom for each node in the Cosserat theory with respect to the classical theory, the finite element computations are less time-consuming for the Cosserat theory. The reason is that the rate at which the finite element computations converges in each increment for the Cosserat theory is faster than for the classical theory. The numbers of iterations necessary for the convergence of the classical and Cosserat theories used for the elastic–plastic analysis of the plate are presented in Table 2. The average number of iterations at each increment is a good measure of convergence rate and the required time for the solution procedure. When the mesh is coarse, say the 8×16 mesh, the convergence rate is approximately the same for both theories. However, as the mesh refines, say the 20×40 mesh, the computational effort used to obtain the Cosserat solution is 15% of the classical solution. For a better comparison of the computational efforts in the Cosserat and classical theories,

Table 2
Comparison of the average number of iterations used for convergence in each increment for classical and Cosserat theories

Mesh divisions	Theory used	Average no. of iterations	Min. no. of iteration	Max. no. of iteration	Variance
8×16	Classic	33	4	65	0.238
	Cosserat	30	2	69	0.253
10×20	Classic	38	4	74	0.256
	Cosserat	8	2	18	0.173
12×24	Classic	43	4	80	0.26
	Cosserat	8	2	18	0.192
20×40	Classic	32	3	73	0.649
	Cosserat	5	2	14	0.279

The value of $\bar{\varepsilon}$ is 1e−4.

Table 2 also reflects the maximum and minimum number of iterations as well as the variance of these values.

In order to solve nonlinear problems, there are two approaches for performing the Newton–Raphson method including the full and modified Newton–Raphson. When the full Newton–Raphson method is employed, the tangent stiffness matrix is updated (and inversed) in all iterations. On the other hand, the tangent stiffness matrix is assembled and inversed only at the beginning of each increment in the case of the modified Newton–Raphson method. Consequently, in the full Newton–Raphson method the convergence is achieved by fewer iterations with greater computational effort. Table 3 presents the average number of iterations at each increment when these two approaches are used for the elastic–plastic analysis of the plate based on the Cosserat theory. When the convergence criterion is satisfied, the solution for displacement and stress fields are approximately the same for both methods. According to this table, the computer time for the modified method is much smaller, though the average numbers of iterations are approximately the same for both methods.

7.2. Effects of the internal length in the Cosserat theory

The Cosserat theory gives better results than the classical theory, though the results obtained by this theory depend on the internal length of the material. According to Fig. 4(b), the force–displacement curves obtained for the internal length of 2 mm with different discretizations of the plate coincide. However, as illustrated in Fig. 6, the force–displacement curves for different discretizations of the same problem do not exactly coincide for the internal length of 1 mm. Thus, decrease of the internal length increases the mesh-dependency of the solution but these results are much better than the classical ones as compared with Fig. 5.

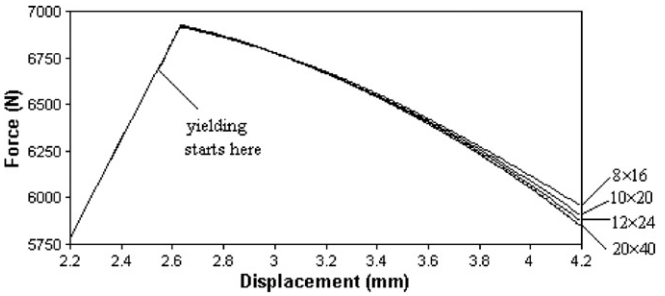

Fig. 6. Force–displacement curves for different discretizations obtained by the Cosserat theory for the internal length of 1 mm.

Fig. 7 shows the plastic zone for different discretizations with the internal length of 0.75 mm. It is noted that the number of elements in the width of the plastic zone are the same for 8×16, 10×20, and 12×24 meshes (the 10×20 mesh is not presented in the figure) but the size of the plastic zone is not the same for these discretizations. On the other hand, the 12×24 and 20×40 meshes have different numbers of plastic elements but approximately the same size of the plastic zone. Accordingly, it is concluded that the mesh-independency of the results in the Cosserat theory is obtained for $l/e \geqslant 0.15$, where e is the element size and the value of 0.15 corresponds to 12×24 mesh. In [1] it has been mentioned that for the mesh-independency of the results in the couple stress theory $l/e \geqslant 0.2$ should be satisfied. Consequently, in order to obtain mesh-independent results by the Cosserat theory, it is not required to use as fine meshes as required by the couple stress theory when the same internal length is used.

Table 3
Comparison of the average number of iterations used for convergence in each increment for full and modified Newton–Raphson methods

Mesh divisions	Type of Newton–Raphson	Average no. of iterations	Min. no. of iteration	Max. no. of iteration	Variance	Computer time (s)
8×16	Full	34	7	62	0.161	312
	Modified	37	12	65	0.138	109
10×20	Full	28	5	43	0.168	484
	Modified	29	10	52	0.145	165
12×24	Full	23	2	37	0.187	480
	Modified	24	9	52	0.178	177
20×40	Full	9	2	27	0.247	1244
	Modified	10	5	27	0.235	600

The value of $\bar{\varepsilon}$ is 1e−5. The values of the computer time are just presented for comparison, though these values depend on the speed of the computer used.

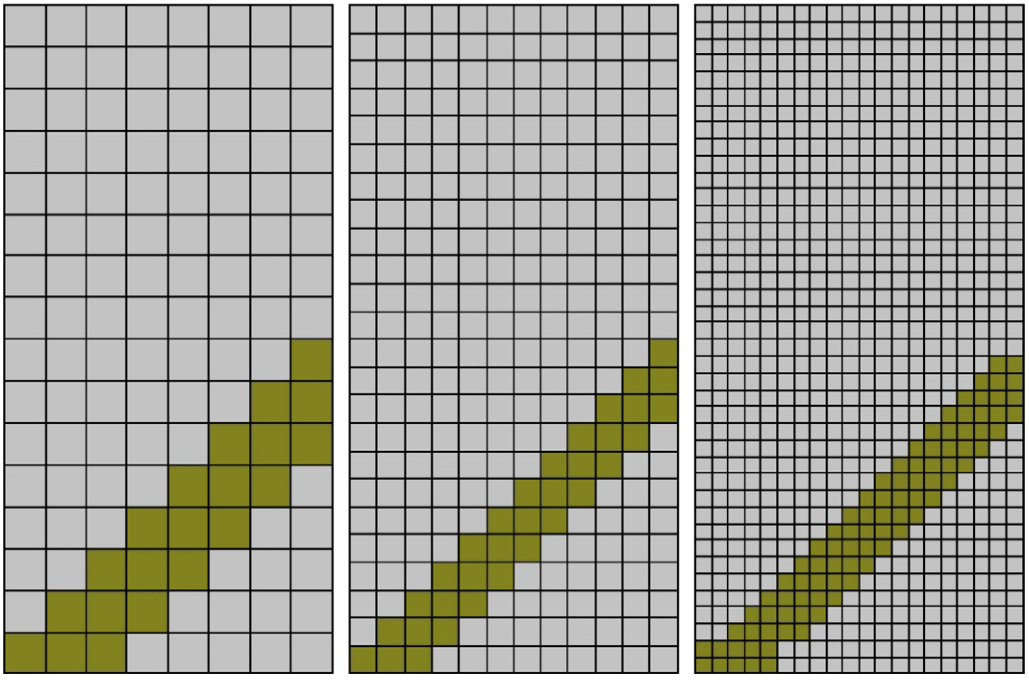

Fig. 7. Plastic zone for the same problem as the one in Fig. 3 except that the internal length is 0.75 mm.

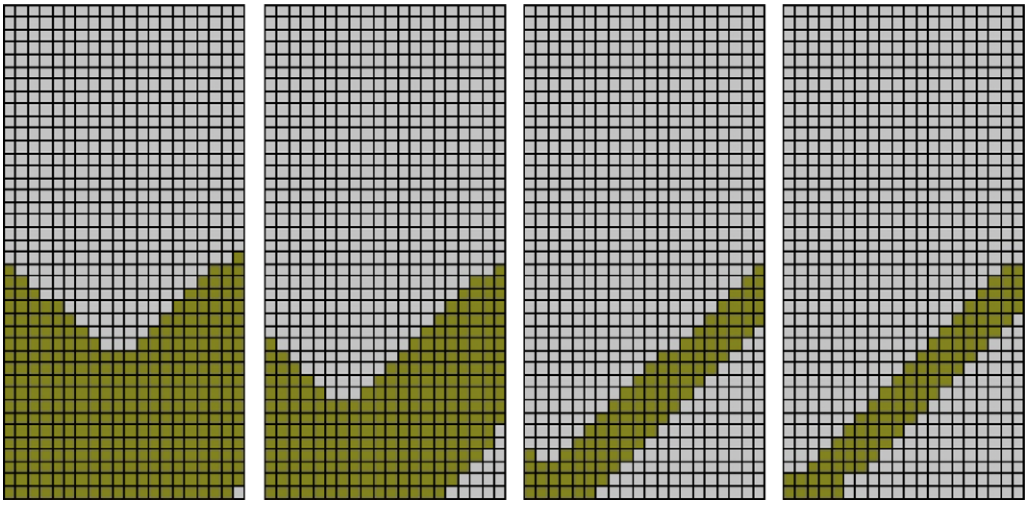

Fig. 8. Plastic zone for different values of the internal length when the discretization is 20×40. The internal lengths are 3, 2, 1, and 0.75 mm, respectively, from left to right and dimensionless Cosserat shear modulus is 0.5.

The internal length greatly affects both the displacement and micro-rotation fields; these fields are smoother for greater values of the internal length. Fig. 8 shows the plastic zone for the 20×40 mesh with different values of the internal length of 0.75, 1, 2, and 3 mm. In general, increase of the internal length expands the plastic zone. In other words, when the internal length increases, the plastic zone expands and finally covers a major part of the body which causes the relief of the localization. In the case of the classical theory, where the internal length is zero, the localized domain vanishes because by refining the discretization the size of the localized domain tends to zero.

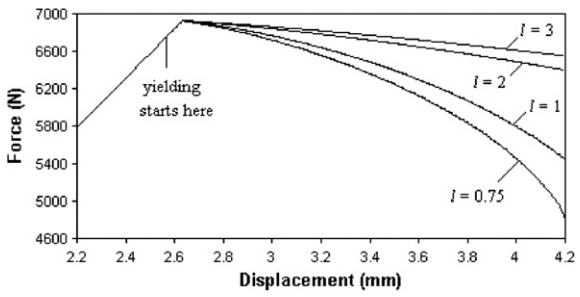

Fig. 9. Force–displacement curves for different internal lengths and 20×40 mesh. The Cosserat parameter a is 0.5.

Table 4
Effect of the internal length on convergence rate for different discretizations when the same convergence tolerance is used

Mesh division	Internal length	Average no. of iterations	Min. no. of iteration	Max. no. of iteration	Variance
8×16	2	37	2	65	0.139
	1	90	12	152	0.292
	0.75	125	12	206	0.227
10×20	2	29	10	52	0.145
	1	87	10	111	0.236
	0.75	119	10	167	0.298
12×24	2	23	9	52	0.178
	1	62	9	111	0.259
	0.75	115	9	180	0.335

The Cosserat parameter a is 0.5.

Since the size of plastic zones obtained based on the Cosserat theory depends on the internal length, it is useful to compare the results with the experimental data for different values of the internal length. As shown in Fig. 8, the localized zone obtained in our work for the internal length of 1 mm is approximately 15 mm wide. Considering the internal length as the average grain size, according to the experimental data provided by Vardoulakis et al. [19], the localized zone for the internal length of 1 mm is of 16 mm width, which is close to the 15 mm predicted by the proposed modeling.

Fig. 9 illustrates the force–displacement curves for different values of the internal length when the 20×40 discretization is used. In accordance with the figure, it is concluded that increase of the internal length results in greater values of predicted reaction force. This may not be what we expect at the first glance; as shown in Fig. 8,

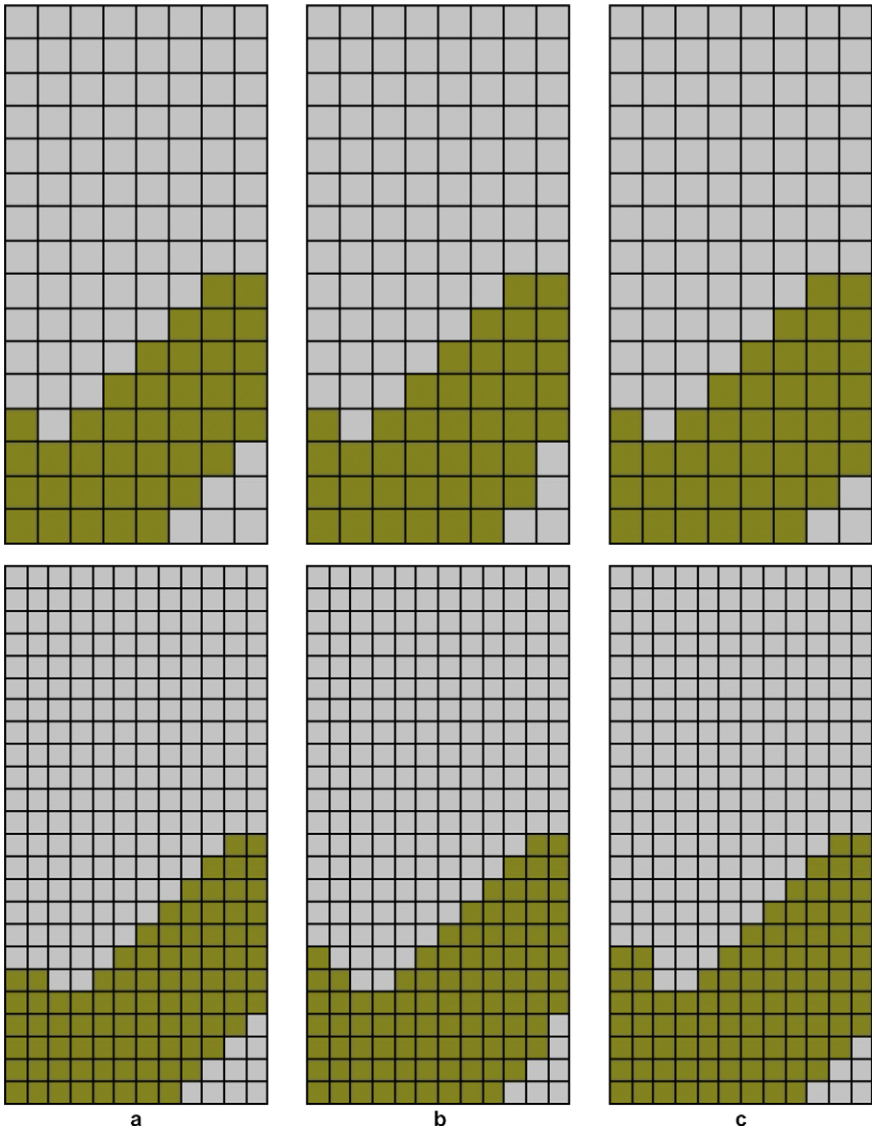

Fig. 10. Plastic regions obtained for three different values of the Cosserat material parameter a when the internal length is 2 mm. (a) $a = 0.5$, (b) $a = 1$, and (c) $a = 3.7$.

the plastic zone is more extensive for larger values of the internal length and since the material has a softening property we expect the reaction force to decrease when the internal length increases. The reason for increase of the reaction force in the softening material lies in the fact that the effective plastic strain is much greater with smaller values of the internal length. The maximum values of the effective plastic strain are 0.096, 0.15, 0.47, and 0.79 for the internal lengths 3, 2, 1, and 0.75 mm with 20×40 discretization, respectively. It is noted that for the classical theory the maximum value of the effective plastic strain is 1.457 for the same discretization.

Table 4 shows the effect of the internal length on the rate of convergence in the elastic–plastic analysis of the plate. As shown in this table, the rate of convergence decreases in the analysis of the plate for smaller values of the internal length. This is predictable since zero internal length corresponds to the classical theory, which is of less convergence rate. Also, the average number of iterations decreases as mesh refines for all values of the internal length. Furthermore, it is concluded that the decrease of the internal length affects convergence more significantly using finer discretizations.

7.3. Effects of the Cosserat material parameter a

Another parameter which appears in the Cosserat theory is the material parameter a, which may be interpreted as the dimensionless Cosserat shear modulus. The value of this parameter has been assumed 0.5 so far in the analyses. Fig. 10 shows the plastic zones obtained by three different values of a with the internal length of 2 mm in the plate. According to the figure, the variation of this parameter has little effect on the plastic zone, though, the plastic zone extends in some parts as parameter a increases. On the other hand, increasing the value of a leads to a decrease in the effective plastic strain; the values of the maximum effective plastic strain are 0.146, 0.141, and 0.138 for $a = 0.5$, $a = 1$, and $a = 3.7$, respectively, when the discretization is 12×24 and the internal length is 2 mm. In the classical theory, where $a = 0$, the maximum effective plastic strain is 0.633 for the same discretization.

Unlike the internal length, the dimensionless Cosserat shear modulus has little effect on the convergence rate and force–displacement curves. The convergence rate is slightly (about 5 percent) more for $a = 1$ when compared with the convergence rate for $a = 0.5$. Furthermore, by increasing the value of a, the predicted force also increases but this increase is too small to be considered.

8. Conclusions

Modeling of the localization phenomena is one major advantage of the Cosserat theory with respect to the classical theory. The Cosserat theory introduces a new degree of freedom for each particle called micro-rotation. Insertion of the micro-rotation into kinematic relations causes the strain tensor to be non-symmetric. In addition, the stress tensor is not symmetric in this theory because of the presence of body couples and couple stresses. Two material parameters including the internal length l and the Cosserat material parameter a also appear in this theory. The insertion of these parameters together with presuming a micro-rotation degree of freedom for each particle, leads to reasonable results in modeling of the localization phenomena, which the classical theory is not capable of modeling them.

The numerical results obtained based on the Cosserat theory show that the theory is capable of reasonable modeling of the localization phenomena. The Cosserat theory gives mesh-independent results. On the other hand, the results of the classical theory are strongly mesh-dependent. A comparison between the results for the localized zones obtained based on the Cosserat theory and those predicted by experimental data shows that they are in good agreement. It is shown that decrease of the internal length increases the mesh-dependency of the solution. Furthermore, the displacement field obtained by the Cosserat theory is smoother than that of the couple stress theory for the same internal length l. For the problems considered here, the mesh-independency of the results based on the Cosserat theory is obtained for $l/e \geqslant 0.15$, and in the couple stress theory for $l/e \geqslant 0.2$, where e is the element size. In other words, for the mesh-independency of the Cosserat theory, it is not required to use as fine meshes as required by the couple stress theory for the same internal length.

The computational efforts required to perform the elastic–plastic finite element analysis is measured in terms of the number of iterations and the computer time for each iteration used in the solution procedure. It has been shown that the average number of iteration is much less for the Cosserat theory compared with the classical theory. The computational effort for the solution procedure is less in the Cosserat theory, in spite of an additional degree of freedom for each node in this theory. Also, comparing the computational efforts of the modified Newton–Raphson and full Newton–Raphson method for the problems considered in this paper, it is concluded that the former is more efficient for the nonlinear finite element analysis based on the Cosserat theory.

References

[1] M. Ristinmaa, M. Vecchi, Use of couple stress theory in elasto-plasticity, Computer Methods in Applied Mechanics and Engineering 136 (1996) 205–224.
[2] H.L. Schreyer, Z. Chen, One dimensional softening with localization, Journal of Applied Mechanics 53 (1986) 791–797.
[3] H. Cramer, R. Findeiss, G. Steinl, W. Wunderlich, An approach to adaptive finite element analysis in associated and non-associated plasticity considering localization phenomena, Computer Methods in Applied Mechanics and Engineering 176 (1999) 187–202.
[4] R. Chambon, D. Caillerie, T. Matsuchima, Plastic continuum with microstructure, local second gradient theories for geomaterials: localization studies, International Journal of Solids and Structures 38 (2001) 8503–8527.
[5] I.S. Pavlov, A.I. Potapov, G.A. Maugin, A 2D granular medium with rotating particles, International Journal of Solids and Structures, in press.

[6] R.D. Mindlin, Stress functions for a Cosserat continuum, International Journal of Solids and Structures (1965) 265–271.
[7] E. Cosserat, F. Cosserat, Theorie des Corps Deformables, Librairie Scientifique, A. Hermann et Fils, Paris, 1909.
[8] H. Neuber, On the general solution of linear-elastic problems in isotropic and anisotropic Cosserat continua, in: Proceedings of the 11th International Congress on Applied Mechanics, Springer, 1965, pp. 153–158.
[9] M. Lazara, H.O.K. Kirchnerb, Cosserat (micropolar) elasticity in Stroh form, International Journal of Solids and Structures 43 (2005) 5377–5398.
[10] M. Baluch, J.E. Goldberg, S.L. Koh, Finite element approach to plane microelasticity, Journal of Structural Divsion – American Society of Civil Engineers 98 (1972) 1957–1964.
[11] S. Nakamura, R. Benedict, R. Lakes, Finite element method for orthotropic micropolar elasticity, International Journal of Engineering Science 22 (1984) 319–330.
[12] E. Providas, M.A. Kattis, Finite element method in plane Cosserat elasticity, Computers and Structures 80 (2002) 2059–2069.
[13] B. Nadler, M.B. Rubin, A new 3-D finite element for nonlinear elasticity using the theory of a Cosserat point, International Journal of Solids and Structures 40 (2003) 4585–4614.
[14] C.S. Jog, Higher-order shell elements based on a Cosserat model, and their use in the topology design of structures, Computer Methods in Applied Mechanics and Engineering 193 (2004) 2191–2220.
[15] M. Cerrolazaa, J. Sulemb, A. Elbiedb, A Cosserat non-linear finite element analysis software for blocky structures, Advances in Engineering Software 30 (1999) 69–83.
[16] S. Diebels, H. Steeb, Stress and couple stress in foams, Computational Materials Science 28 (2003) 714–722.
[17] O.C. Zienkiewicz, R.L. Taylor, fourth ed., The Finite Element Method, vol. 1, McGraw-Hill, 1989.
[18] M.A. Crisfield, Non-linear Finite Element Analysis of Solids and Structures, Wiley publication, 1991.
[19] I. Vardoulakis, B. Graf, A. Hettler, Shear-band formation in a fine-grained sand, Proceedings of the 5th International Conference on Numerical Methods in Geomechaincs, vol. 1, Balkema, Nogaya, Rotterdam, 1985, pp. 517–521.